Sol-gel synthesis, characterization of ZnO thin films on different substrates, and bandgap calculation by the Tauc plot method

D. Parajuli[1,2,*], **Sandip Dangi**[1], **Bhumi Raj Sharma**[3]
Nunu Lal Shah[1], **Devendra KC**[4]

[1]*Department of Physics, Tri-Chandra Multiple Campus, Ghantaghar, Kathmandu*
[2]*Research Center for Applied Science and Technology, Tribhuvan University, Kirtipur*
[3]*Department of Physics, Janapriya Multiple Campus, Pokhara, Kaski*
[4]*Myrveien 13, 9740 Lebesby, Norway*

*Corresponding author. Email: deepenparaj@gmail.com

Abstract

The sol-gel spin coating method was used for the preparation of the Zinc Oxide which was coated over polymer, transparent, and glass translucent substrates and characterized with the help of a UV-Vis Spectroscope. The wavelength bandgap of those samples was found to be 296nm, 310.5nm, and 330nm respectively. The actual band gap of ZnO is 388nm. Similarly, their optical bandgap energy calculated by the Tauc Plot method were 3.641eV, 3.385eV, and 3.495 eV respectively. The transparent polymer slide has the lowest wavelength bandgap and the translucent glass slide has the highest. Further, the bandgap's value differs from its actual value to the difference in the absorption process due to the presence of the substrate. These results suggest that the choice of substrate can significantly impact the optical properties and performance of the zinc oxide thin film. This result can be applied in developing and optimizing zinc oxide thin films for various purposes, such as in solar cells, sensors, and optoelectronics. By carefully selecting the substrate, it may be possible to tailor the bandgap energy and other optical properties of the thin film to better suit the specific application.

1 Introduction

Extensive research is conducted these days on metal oxides in nanoparticle form due to their diverse potential applications in various fields, such as agriculture, medicine, industry, and technology. The metal oxides being researched include copper, zinc, tin, magnesium, zirconium, silver, titanium, cerium, and others. Among these, zinc oxide (ZnO) is particularly important due to its electronic and

optical properties, radiation stability, low cost of production, and non-toxicity. It has a high bandgap of 3.37 eV at room temperature and is commonly used in semiconducting oxide thin films, which are extensively utilized in solar cells, sensors, LEDs, surface acoustic devices, cosmetics, and paintings. Previously, a study was conducted on sol-gel synthesized ZnO deposited on a glass slide [1] which will be studied further with other options in this work. ZnO is also utilized in organic and solar hybrid cells [2–5] in the form of a buffer layer for the cathode buffer layer, and it performs efficiently in both bulk and 2D forms, with thin films proving more effective than bulk ones. Due to its versatility and various uses, ZnO is produced on a large scale [6] these days. ZnOs are typically N-type with a wide bandgap of 3.37 eV [7] and have bands in the UV and visible light regions [8]. During the growth process, the interstitial sites, vacancies, or anti-sites of oxygen, zinc, and other factors may affect the final product's parameters. ZnO's point defect has an electron mobility of approximately 300 cm^2 V^{-2} s^{-1} for bulk ZnO and around 1000 cm^2 V^{-2} s^{-1} for ZnO NSs, increasing the capacity for electron transfer. Additionally, ZnO is active in oxidation and reduction processes. However, ZnO only has the capacity to absorb UV radiation, which is a narrow window of electromagnetic radiation and is difficult to excite the electron-hole pair. Moreover, it can be scratched by light and decompose in higher and lower pH-valued solvents [9]. It can dissolve in highly acidic or basic media under proper biasing [10]. However, the limitations of ZnO can be overcome by using a composite of ZnO with other metals, such as doping, as described in previous literature. There are many processes for the preparation of nanomaterials [11–17]. The thin film ZnO [18] can be prepared with different methods like a deposition [19], sol-gel [20], vacuum evaporation [21], sputtering [22,23], Successive Ionic Layer Adsorption and Reaction (SILAR) [24], pyrolysis [25], etc. We have incorporated the simplest but well-controlled stoichiometry [26], method

called sol-gel followed by spin coating [27]. The sol-gel method as shown in Figure 2 uses metal alkoxides M (OR)n [derived from weak acids R-OH] and alkoxysilanes for their reaction in radial or all direction [28]. We have taken Zn (NO$_3$)$_2$ for ZnO synthesis [29]. The substrate for coating was transparent glass, translucent glass, and polymer slide. They were examined under a UV Vis spectroscope. For spin coating, the substrate is mounted on a rotating system (10,000 rpm) whose centrifugal force spread the ZnO solution uniformly around the slide against surface tension and viscous force thereby creating the thin film of micro to the nanometer range. It is not effective for samples with a large area of the substrate. Only 5% of the sample is distributed over the slide and the rest 95% is flung off [30]. The thickness of the sample is dependent on various parameters and given:

$$ h = \left(1 - \frac{\rho_A}{\rho_{A0}}\right) \left(\frac{2\eta m}{2\rho_{A0}\omega^2}\right)^{\frac{1}{3}} \tag{1} $$

where,ρ , η, M, and ω are the density, viscosity, evaporation rate, and angular speed of the slide respectively.

The slides can be systematically coated [30]. The Tauc plot method was used to calculate the band gap energy in which the energy is on the x-axis and $(\alpha h\nu)^2$ on the y-axis. A tangent line on the curve at $\alpha = 0$ touches a point on the x-axis is the optical bandgap energy of the materials. To get the curve first, we have to begin the Tauc plot. The equation $(\alpha h\nu)^2 = K(h\nu - E_g)$ is known as Tauc and Davis-Mott relation [31]. This relation is used to find the optical bandgap energy of a thin film of zinc oxide from UV-V is absorption spectroscopy. In this equation, α is the absorption coefficient '$h\nu$' is the incident photon energy, K is the energy-independent constant and E_g is the optical band gap energy of the zinc oxide. In this equation, 'n' represents the nature of the transition. For direct gap semiconducting material, n=2.
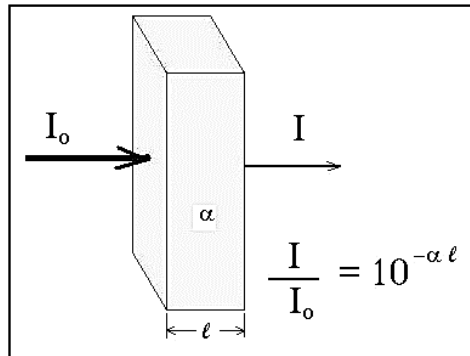

Figure 1: The Beer Lambert's Law.

In UV-V is spectroscopy, the data which is given to us have wavelength and absorbance. Therefore, we have to convert wavelength to energy and need to calculate the absorbance coefficient (α) from absorbance data. We use the Max Planck equation energy from wavelength, i.e.

$$E_g = h\nu \tag{2}$$

Where h is Planck's constant and ν is the frequency of UV-Vis light incident on the substrate in which the thin film of zinc oxide is coated. We know that,

$$\nu = \frac{c}{\lambda} \tag{3}$$

Putting equation (2) in equation (1),

$$E_g = \frac{hc}{\lambda} \tag{4}$$

where c is the speed of light and putting the values in equation (4), we get,

$$E_g = \frac{6.62 \times 10^{-34} Js \times 3 \times 10^8 m/s}{\lambda}$$

$$E_g = \frac{19.854 \times 10^{-26} Jm}{\lambda} \tag{5}$$

In equation (4) the energy is in joule, we have to convert it into electron volts. We know, $1eV = 1.602 \times 10^{-19} J$, therefore energy in equation (4) can be converted as follows:

$$E_g = \frac{19.854 \times 10^{-26} eVm}{1.602 \times 10^{-19} \lambda}$$

$$E_g = \frac{12.393 \times 10^{-7} eVm}{\lambda}$$

where $10^{-9} m = 1 nm$

$$E_g = \frac{12393\ eVnm}{\lambda} \tag{6}$$

In equation (6), we have to put the value of the wavelength in the nanometer obtained from the UV- V is spectroscope when UV-V is light incident in zinc oxide. In this project work, we have used origin software to convert wavelength to energy with help of equation (6) which can be seen in Figure 1. The coefficient of absorption (α) is obtained by plotting $(\alpha h\nu)^2$ on the y-axis where '$h\nu$' is the incident photonic energy. Using Beer Lambert's law, we can calculate 'α' from absorbance data [32, 33].

In Figure 1, I is the intensity of transmitted light, I_o is the intensity of incident light, 'α' is the absorption coefficient and l is the path length in which absorbance takes place. From Beer Lambert's equation,

$$I = I_O e^{-\alpha l} \tag{7}$$

We can modify equation (7) as

$$\frac{I}{I_0} = e^{-\alpha l}$$

Taking logs on both sides,

$$log\frac{I}{I_0} = log e^{-\alpha l}$$

$$log\frac{I}{I_0} = -\alpha l\, log e$$

$$log\frac{I_0}{I} = \alpha l\, log e$$

As we know,

$$Absorbance(A) = log\frac{I_0}{I}$$

So we can write as,

$$A = \alpha L\, log e$$

$$\alpha = A\frac{1}{L\, log e}$$

where, $log e = 0.4343$, then we can write,

$$\alpha = A\frac{1}{0.4343 L}$$

$$\alpha = 2.302 \times \frac{A}{L}$$

As we took the thin film of zinc oxide so the path length = 10mm = 1cm

$$\alpha = 2.302 \times \frac{A}{1cm}$$

$$\alpha = 2.302 \times A cm^{-1} \tag{8}$$

The unit of absorbance coefficient would be cm^{-1} because 2.303 is a constant and Absorption is a dimensionless quantity.

Thus using equation (7), the absorption coefficient is calculated with the help of origin software which can be seen in Figure 1.

Now combining equation (7) with energy to get our desire Tauc relation i.e.
$(\alpha h\nu)^n = $ (Absorption coefficient $\times$ energy)^n

$$(\alpha h\nu)^n = (2.303 \times A \times h\nu)^n \tag{9}$$

Equation (9) gives the value of $(\alpha h\nu)^2$ with the unit $(eV cm^{-1})^2$. Then, a graph is plotted with energy $(h\nu/\lambda)$ on the x-axis and $(\alpha h\nu)^2$ on the y-axis. Then, draw a tangent line on the curve where $\alpha=0$. The point where it touches the axis is the optical bandgap energy of the materials.

2 Materials and Methods

The work mainly can be divided into three parts: 1) to obtain a thin film of zinc oxide by the sol-gel method and 2) analysis of the zinc oxide coated thin films over different glass slides using UV-V is spectroscope, and 3) calculation of the optical band gap energy of a thin film of zinc oxide with the help the Tauc plot method. Steps 1 and 2 are schematically shown in Figure 2. The preparation of ZnO solution in the laboratory of RECAST, TU is shown in figures 3-13. The reaction taken in preparing ZnO is shown in the following reaction: $Zn\ (NO_3)_2 + CH_2CH\ (OH) \rightarrow ZnO + CH_2CH\ (OH) + 2NO_2 + O$

In this work, the slides can be cleaned by keeping them in the solution of water and detergent for 1hr 30 minutes followed by distilled water washing, ethanol, and acetone. The slides are then dried in a hot air oven for the complete removal of moisture from the surface. We have used polyvinyl alcohol (PVA) as a chelating agent and zinc nitrate as a precursor for the production of zinc oxide nanoparticles. At first, 1 ± 0.05 gm of PVA was mixed with 100ml of distilled water and stirred at 80^0C for 45 minutes in a magnetic stirrer. Next, zinc nitrate of 2.974 ± 0.05gm in 100ml of pure distilled water and stirred in a magnetic stirrer. An equal volume (20ml) of each solution is mixed and stirred in a magnetic stirrer at room temperature (23^0C while experimenting) for 3hrs of time duration. The solution was again stirred for the next 5 hrs. at 50^0C to form a thick hot solution. Cooled to room temperature to obtain a gel solution. Then, we added a few drops of methanol help of a volumetric pipette and stirred for the next 15 min at normal temperature to get the clear gel-type solution. The gel solution was coated over the clean glass slide by keeping a few droplets of the gel-type clear solution over the spin coater (we have used the CPU 12V DC fan as the spin coater which can be seen in Figure 10) and spinner for the next 50 second. The resulting slide was heated for 10 minutes at 2000C in a preheated hot air oven and cool them to room temperature. The systematic diagram of the sol-gel synthesis of zinc oxide over a glass slide is given in Figure 2. Then, obtained thin film of zinc oxide is analyzed with the help of a UV-Vn is spectroscope.
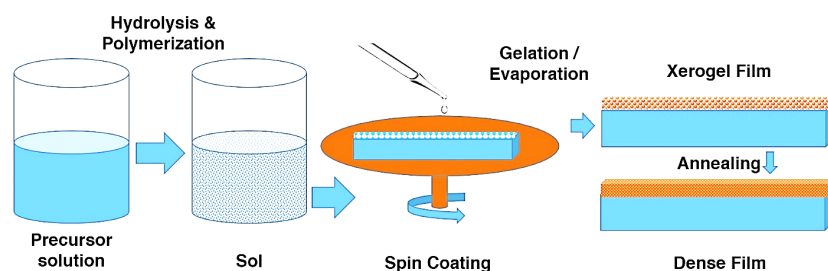

Figure 2: A schematic view of the sol-gel process for the ZnO thin film processing.

Figure 3: Dissolving PVA with distilled water at 80^oC.

Figure 4: Mixing PVA and Zinc nitrate solution.

Figure 5: Stirring the mixed solution for 3 hrs.

Figure 6: Stirred continued for 5hrs. at 50°C.

Figure 7: Normal temperature solution preparation.

Figure 8: Adding methanol and stir the solution for 15 minutes.

Figure 9: Formation of Clear Gel solution.

Figure 10: Coating gel over the slide to get a thin film.

Figure 11: Heating the coated thin film at 200°C in a hot air oven.

Figure 12: Thin film of Zinc Oxide.

Figure 13: ZnO-coated transparent and translucent glass/polymer slide .

3 Results and Discussion

3.1 XRD study

The X-ray diffraction (XRD) pattern in Figure 14 displays the crystallographic planes (100), (002), (101), (102), (110), (103), (200), (112), (201), (004), and (202) at θ values of 31.76^0, 34.44^0, 36.24^0, 47.56^0, 56.66^0, 62.90^0, 66.42^0, 67.96^0, 69.14^0, 72.64^0, and 76.98^0, respectively, which matches with the JCPDS card number 01-089-1397 [20, 34, 35] The presence of sharp and narrow peaks indicates that the ZnO NPs are highly crystalline. Furthermore, the sample exhibits a single-phase Wurtzite structure, which is a hexagonal close-packed crystal structure commonly observed in ZnO [25].

The average crystallite size is obtained with the help of Sherrer's $D = \dfrac{k\lambda}{\beta\cos\theta}$ formula,, Where D is the particle size of the ZnO, K is the shape factor whose value varies from 0.89 to 0.94 and 0.94 is chosen for spherical NPs, is the wavelength of the Cu–K radiations (1.5406) used in the X–ray diffraction, β is the full-width half maximum (FWHM), and θ is the Bragg's angle of different peaks. The average particle size of the ZnO nanoparticle was found at 39nm. The particle size and strain can induce the broadening of the XRD peaks.

3.2 SEM Study

The Scanning Electron Microscope (SEM) image of a pure ZnO crystal is shown in Figure 15 where oxygen and zinc atoms are represented by large and smaller spheres. The morphology of the composition agrees well with the previous literature [36].
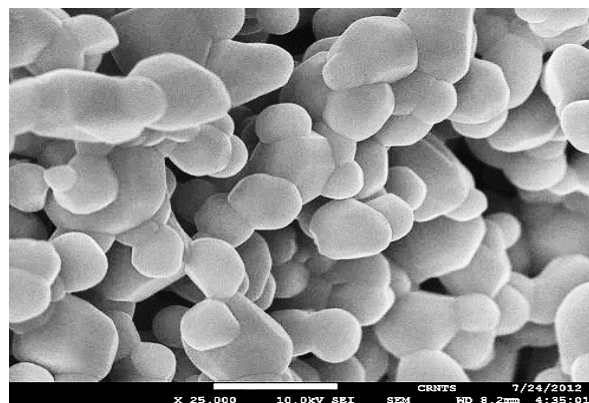

Figure 14: X-ray diffraction (XRD) patterns of Zinc oxide nanoparticles.

Figure 15: TSEM Image of ZnO nanoparticles.

3.3 UV- V is spectroscope study

UV-Visible spectroscopy is an analytical technique used to measure the absorption or transmission of discrete wavelengths of UV or visible light by a sample, compared to a reference or blank sample. This method is suitable for both organic and inorganic compounds, and the pattern observed in the spectroscopic data depends on the reflective or absorptive properties of the sample. UV spectroscopy is simple, versatile, cost-effective, and nondestructive. Spectrophotometers are used to measure the absorption or transmission of light as a function of the wavelength that passes through a sample. However, exposure to UV light can damage organic samples, which is a potential risk associated with this technique. To better understand how a UV-Vis spectrophotometer works, it is essential to consider its main components. Several variations of the instrument exist, but a typical system usually includes a light source, a monochromator, a sample holder, a detector, and a data acquisition system, as illustrated in Figure 16. The light source generates the UV or visible light, and the monochromator selects specific wavelengths. The sample holder holds the sample in place and ensures uniform exposure to light, while the detector measures the amount of light absorbed or transmitted by the sample. Finally, the data acquisition system records the spectral data, which can be analyzed to determine the properties of the sample.
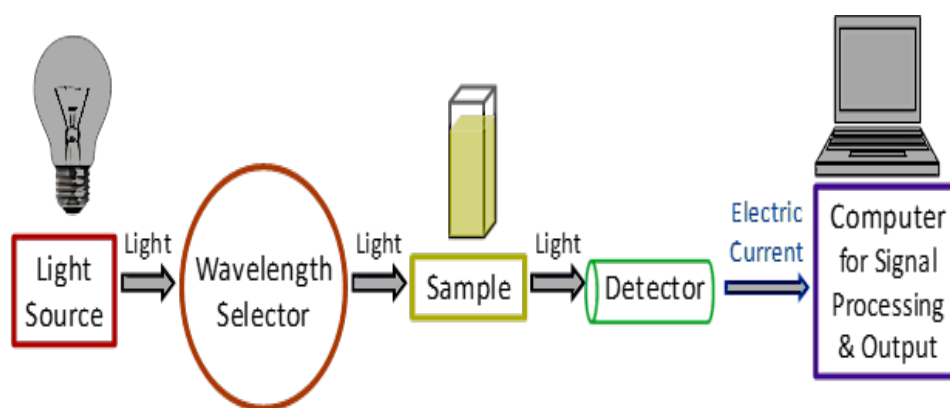

Figure 16: A simplified schematic of the main components in a UV-Vis spectrophotometer [37].

In this process, a steady source of light like a Xenon lamp is needed for UV and visible light range. A deuterium lamp is used for the UV light range. A tungsten or halogen lamp is needed for visible range. The determination wavelength range needed for the substrate material, the uncoated substrate is taken as the sample and identified as the baseline wavelength and was found to be in the range 190-600 nm for UV characterization. A wavelength selector is used in the spectrophotometer to set the wavelength in its baseline range. Then the light of a wavelength within the baseline range is passed through the coated sample and characterized with respect to a reference uncoated sample.

In this work, we developed a thin film of zinc oxide over 1) transparent glass slides, 2) translucent glass slides, and 3) transparent polymer slides as in Figures 12 and 13 respectively.

Their optical properties were studied with a UV visible spectrometer and calculated their bandgap energy with the help of the Tauc plot method as follows:

3.3.1 UV-V is spectroscopy for transparent polymer slide

The spectrum obtained from UV-Visible spectroscopy (figure 17) shows a maximum peak at 296nm, as the bandgap wavelength of ZnO. However, the actual bandgap wavelength of the bulk ZnO is reported to be 388nm [38–40]. This discrepancy may be attributed to the use of substrates that diminish the absorption of radiation. Further, the nanograin of the different substrates differs in the value of the optical energy band [41–43]. In contrast, the uncoated transparent polymer slide showed no such peak as seen in Figure 18. Further, the Tauc plot method was used to calculate the bandgap energy of zinc oxide coated on a transparent polymer slide, yielding a value of 3.77eV, as illustrated in the corresponding Figure 19.
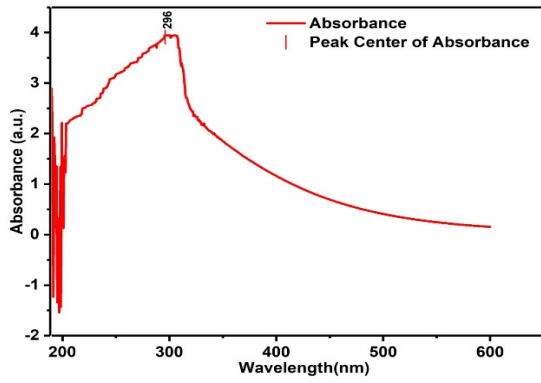
Figure 17: UV-Visible spectrum of a thin film of zinc oxide coated over a transparent polymer slide.
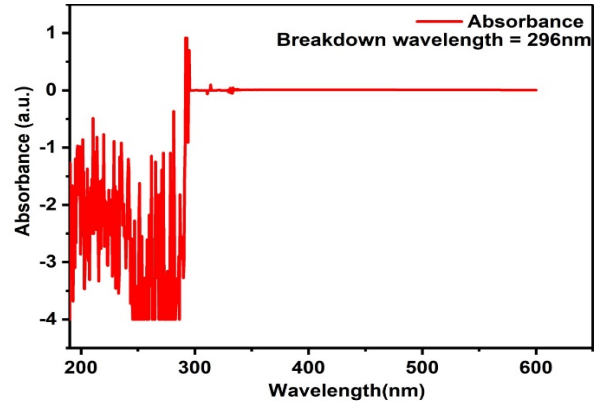
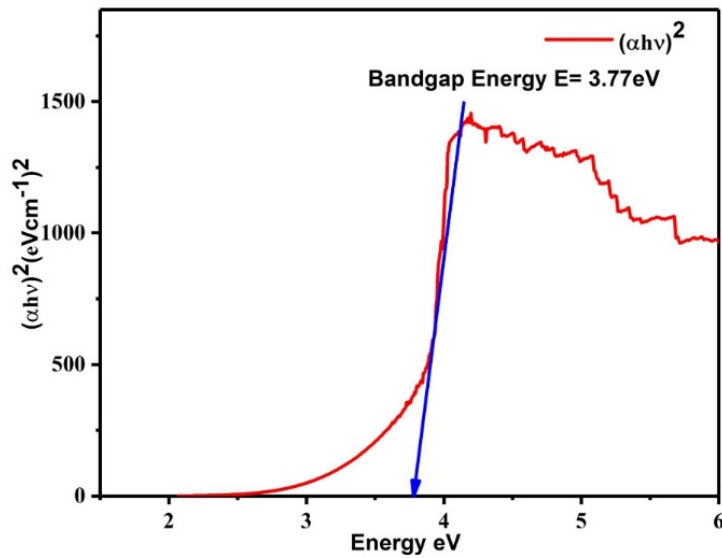Figure 18: UV-Visible spectrum of uncoated over transparent polymer slide.

Figure 19: The optical absorption coefficient (hv)2 of zinc oxide-coated transparent polymer slide as a function of the photon.
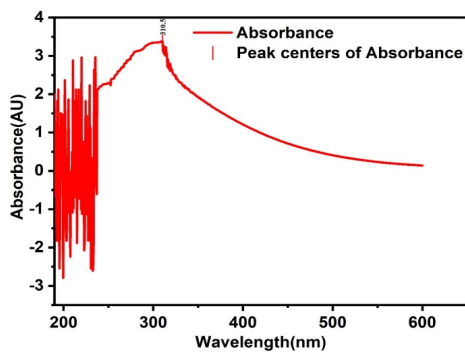

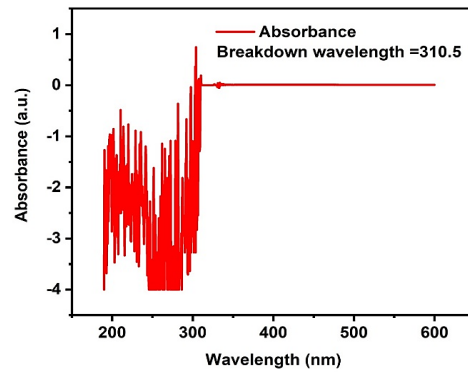Figure 20: UV-Visible spectrum of a thin film of zinc oxide coated over a transparent glass slide.

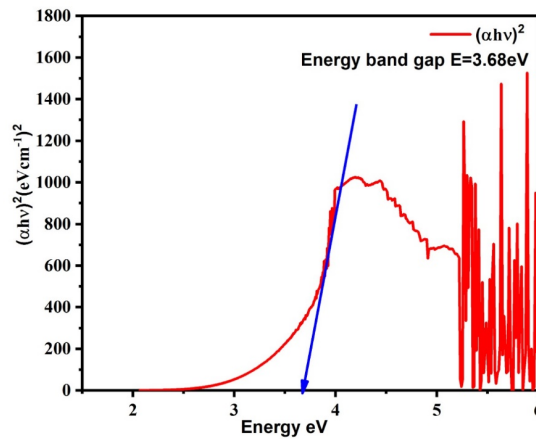Figure 21: UV-Visible spectrum of uncoated over a transparent glass slide.

Figure 22: The optical absorption coefficient (hv)2 of zinc oxide-coated transparent glass slide as a function of the photon.

3.3.2 UV-Vis spectroscopy for transparent glass slide

The UV-Visible spectrum as in Figure 20 indicates that the maximum peaks are located at 310.5nm as the band gap wavelength of ZnO. However, it is important to note that the actual band gap wavelength of bulk ZnO nanoparticles is 388nm [38–40], which is higher than the measured value. This discrepancy may be due to the substrate materials used for coating zinc oxide, which reduced the absorption of radiation. Further, the nanograin of the different substrates differs in the value of the optical energy band [41–43]. In contrast, Figure 21 shows no such peak for the uncoated transparent polymer slide, and the deflection begins at a wavelength of 310.5nm. The bandgap energy of the zinc oxide coated over a transparent glass slide was calculated with the help of the Tauc plot method and found 3.68eV as in Figure 22.
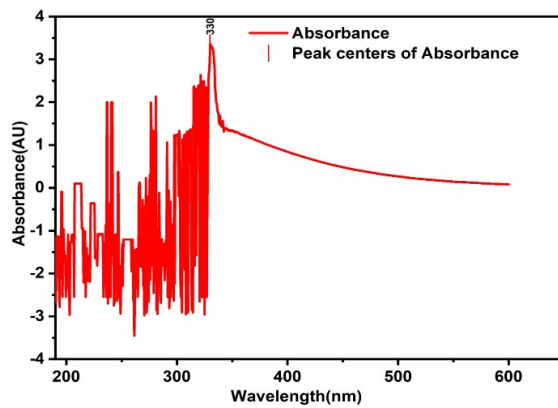

Figure 23: UV-Visible spectrum of a thin film of zinc oxide coated over a translucent glass slide.
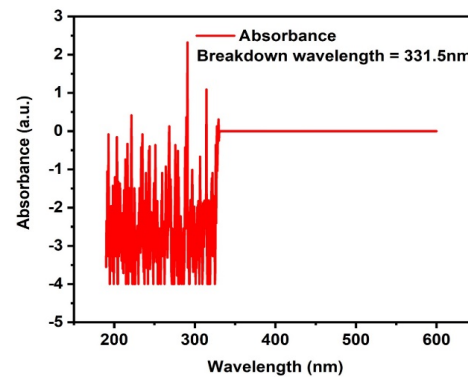

Figure 24: UV-Visible spectrum of uncoated translucent glass slide.

3.3.3 UV-V is spectroscopy for translucent glass slide

The UV-Visible spectrum displayed in Figure 23 reveals that the maximum peaks are observed at a wavelength higher than 331.5nm. However, the actual band gap wavelength of ZnO nanoparticles is known to be 388nm [38–40], which is higher than the measured value. This difference in the measured and actual values may be attributed to the sub-
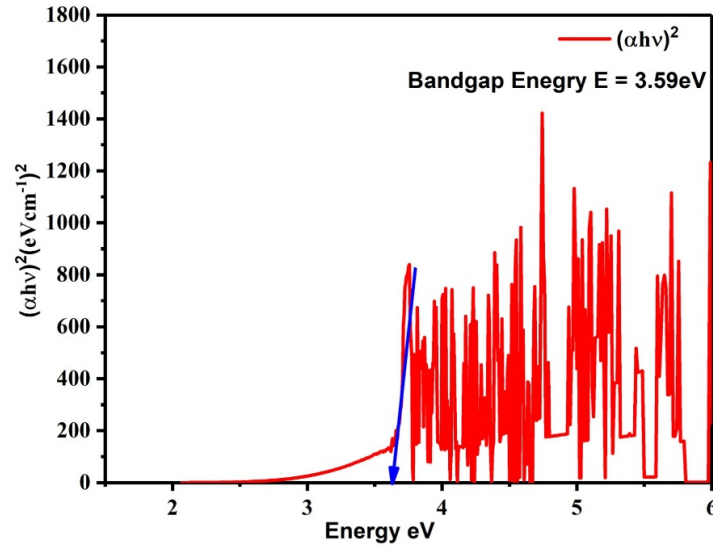
Figure 25: The optical absorption coefficient (hv)2 of zinc oxide-coated translucent glass slide as a function of the photon.

strate materials used for coating zinc oxide affecting the absorption processes of radiation. Further, the nanograin of the different substrates differs in the value of the optical energy band [41–43]. Conversely, Figure 24 shows no such peak for the uncoated transparent polymer slide, and the deflection initiates at a wavelength of 331.5nm. The bandgap energy of the zinc oxide over a transparent polymer slide was found to be 3.59eV with the help of the Tauc plot method as in Figure 25. The actual wavelength, Peak Wavelength, and Optical bandgap of ZnO thin film for different substrates are listed in Table 1 and the computational values of ZnO are listed in Table 2.

Table 1: Actual wavelength, Peak Wavelength, and Optical bandgap of ZnO thin film for different substrate.

	Transparent Polymer	Transparent Glass	Translucent Glass
Peak Wavelength (nm) with a substrate	296	310.5	331.5
Bandgap energy (eV)	3.77	3.68	3.59
Actual wavelength of ZnO without substrate (nm) [38–40]	388	388	388

Table 2: Computational values of ZnO with different models.

Computational Values of ZnO Bandgap [44]	3.39 (HSE)	3.57 eV GW	3.30eV ZnO Wurtzite

4 Conclusion

The thin films of zinc oxide over different substrates were developed with the sol-gel spin coating method and characterized with the help of a UV-V is spectroscope. The wavelength bandgap of each substrate such as 296nm (polymer substrate), 310.5nm (for transparent glass substrate), and 331.5nm (for translucent glass substrate), and the band energy of zinc oxide coated over the different substrates is 3.77eV (transparent polymer slide), 3.68eV (transparent glass slide), 3.59 eV (translucent glass slide).

The transparent polymer slide has the lowest wavelength bandgap and the translucent glass slide has the highest. The Tauc plot method was used to calculate the bandgap energy. These results suggest that the choice of substrate can significantly impact the optical properties and performance of the zinc oxide thin film. The result is that the polymer is more transparent than the glass. So, we can incorporate polymers where more transparency is needed. This result can be applied in developing and optimizing zinc oxide thin films for various

purposes, such as in solar cells, sensors, and opto-electronics. By carefully selecting the substrate, it may be possible to tailor the bandgap energy and other optical properties of the thin film to better suit the specific application.

References

[1] M. J. Akhtar, M. Ahamed, S. Kumar, M. A. Majeed Khan, J. Ahmad, and S.A. Alrokayan. Zinc oxide nanoparticles selectively induce apoptosis in human cancer cells through reactive oxygen species. *International journal of nanomedicine*, 7:845, 2012.

[2] W. Q. Peng, S.C. Qu, G.W. Cong, and Z. G. Wang. Structure and visible luminescence of zno nanoparticles. *Materials Science in Semiconductor Processing*, 9:156, 2006. 10.2147/IJN.S29129

[3] D. K. Shah, D. KC, D. Parajuli, M. S. Akhtar, C. Y. Kim, and O.-B. Yang. A computational study of carrier lifetime, doping concentration, and thickness of window layer for gaas solar cell based on al2o3 antireflection layer. *Solar Energy*, 234:330, 2022. 10.1016/j.solener.2022.02.006

[4] D. Parajuli, D. K. Shah, D. KC, S. Kumar, M. Park, and B. Pant. Influence of doping concentration and thickness of regions on the performance of ingan single junction-based solar cells: A simulation approach. *Electrochem*, 3:407, 2022. 10.3390/electrochem3030028

[5] D. Parajuli, V. Bhandari, D. KC, A. Thapaliya, A. Subedi, A. Dhakal, S. Dangi, R. Koirala, and M. Bhatta. Numerical approach of single-junction ingan solar cell affected by carrier lifetime and temperature. *Pragya Darshan* , 5:58, 2023. 10.3126/pdmdj.v5i1.52309

[6] Y. Aoun, B. Benhaoua, B. Gasmi, and S. Benramache. Structural, optical and electrical properties of zinc oxide thin films deposited by a spray pyrolysis technique. *Journal of Semiconductors*, 36:013002, 2015. 10.1088/1674-4926/36/1/013002

[7] O. M. Alfano, D. Bahnemann, A. E. Cassano, R. Dillert, and R. Goslich. Photocatalysis in water environments using artificial and solar light. *Catalysis Today*, 58(2-4):199–225, 2000. 10.1016/S0920-5861(00)00252-2

[8] P. G Parejo, M. Zayat, and D. Levy. Highly efficient uv-absorbing thin-film coatings for protection of organic materials against photodegradation. *Journal of Materials Chemistry*, 16(22):2165–2168, 2006. 10.1039/B601577H

[9] P. Banerjee, S. Chakrabarti, S. Maitra, and B. K. Dutta. Zinc oxide nano-particles – sonochemical synthesis, characterization and application for photo-remediation of heavy metal. *Ultrasonics Sonochemistry*, 19(1):85–92, 2012. 10.1016/j.ultsonch.2011.05.007

[10] C. Bayram, R. McClintock, S. Kaya, and M. Razeghi. Engineering future light emitting diodes and photovoltaics with inexpensive materials: Integrating zno and si into gan-based devices. In *Optoelectronic Materials and Devices VII*, volume 8626, page 86260G. International Society for Optics and Photonics, 2013. 10.1117/12.2009999

[11] D. Parajuli and K. Samatha. Structural analysis of cu substituted niin ni-zn ferrite. *BIBECHANA*, 18(1):128–134, 2021. 10.3126/bibechana.v18i1.29475

[12] D. Parajuli and K. Samatha. Morphological analysis of cu substituted niin ni-zn ferrites. *BIBECHANA*, 18(2):80–85, 2021. 10.3126/bibechana.v18i2.34383

[13] D. Parajuli, N. Murali, and K. Samatha. Correlation between the magnetic and dc resistivity studies of cu substituted ni and zn in ni-zn ferrites. *BIBECHANA*, 19(1-2):61, 2022. 10.3126/bibechana.v19i1-2.46387

[14] D. Parajuli, N. Murali, and K. Samatha. Structural, morphological, and magnetic properties of nickel substituted cobalt zinc nanoferrites at different sintering temperature. *J. Nepal Phys. Soc.*, 7(2):24, 2021. 10.3126/jnphyssoc.v7i2.38619

[15] D. Parajuli, V. K. Vagolu, K. Chandramoli, N. Murali, and K. Samatha. Electrical properties of cobalt substituted nzcf and zncf nanoparticles prepared by the soft synthesis method. *J. Nepal Phys. Soc.*, 8(4):45, 2022. 10.3126/jnphyssoc.v7i4.42926

[16] D. Parajuli, V. K. Vagolu, K. Chandramoli, N. Murali, and K. Samatha. Soft chemical synthesis of nickel-zinc-cobalt-ferrite nanoparticles and their structural, morphological and magnetic study at room temperature. *J. Nepal Phys. Soc.*, 7(1):14, 2021. 10.3126/jnphyssoc.v8i1.48281

[17] D. Parajuli, V. K. Vagolu, K. Chandramoli, N. Murali, and K. Samatha. Co-precipitation

synthesis of zncf nanoparticle and their structure, morphological, and magnetic properties characterization. *J. Nepal Phys. Soc.*, 8(3):22, 2022.
10.3126/jnphyssoc.v8i3.50726

[18] K. Chandramouli, B. Suryanarayana, T. A. Babu, V. Raghavendra, D. Parajuli, N. Murali, V. Malapati, T. W. Mammo, P. S. V. Shanmukhi, and U. R. Gudla. Synthesis, structural and antibacterial activity of pure, fe doped, and glucose capped zno nanoparticles. *Surfaces and Interfaces*, 26:101327, 2021.
10.1016/j.surfin.2021.101327

[19] T. David, S. Goldsmith, and R. L. Boxman. Electro-optical and structural properties of thin zno films, prepared by filtered vacuum arc deposition. *Thin Solid Films*, 447–448:61–66, 2004.
10.1016/j.tsf.2003.09.023

[20] J. F. Muth, R. M. Kolbas, A. K. Sharma, S. Oktyabrsky, and J. Narayan. Excitonic structure and absorption coefficient measurements of zno single crystal epitaxial films deposited by pulsed laser deposition. *Journal of Applied Physics*, 85:7884–7889, 1999.
10.1063/1.370601

[21] M. Saravanakumar, S. Agilan, and N. Muthukumarasamy. Effect of annealing temperature on characterization of zno thin films by sol-gel method. *Int. J. Chem Tech Res. Coden*, 6, 2014.

[22] K. B. Sundaram and A. Khan. Characterization and optimization of zinc oxide films by rf magnetron sputtering. *Thin Solid Films*, 295:87–93, 1997.

[23] M. Tomar, V. Gupta, K. Sreenivas, and A. Mansingh. Temperature stability of zno thin film saw device on fused quartz. *IEEE Transactions on Device and Materials Reliability*, 5:494–498, 2005.
10.1109/TDMR.2005.853453

[24] T. L. Yang, D. H. Zhang, J. Ma, H. L. Ma, and Y. Chen. Transparent conducting zno: Al films deposited on organic substrates deposited by rf magnetron-sputtering. *Thin Solid Films*, 326:60–63, 1998.
/10.1016/S0040-6090(98)00763-9

[25] J. H. Lee and B. O. Park. Characteristics of al-doped zno thin films obtained by ultrasonic spray pyrolysis: Effects of al doping and an annealing treatment. *Materials Science and Engineering: B*, 106:242–246, 2004.
10.1016/j.mseb.2003.09.040

[26] N. J. Awang, M. Aziz, and A. R. M. Yusoff. Sol-gel preparation and characterization of zno dopped thin solid films substrates for solar cell. *Solid State Science and Technology*, 16:45–53, 2008.

[27] R. W. Schwartz. Chemical solution deposition of perovskite thin films. *Chemistry of Materials*, 9:2325–2332, 1997.
10.1021/cm970286f

[28] L. Shi, D. S. Shang, Y. S. Chen, J. Wang, J. R. Sun, and B. G. Shen. Improved resistance switching in zno-based devices decorated with ag nanoparticles. *Journal of Physics D: Applied Physics*, 44:455305, 2011.
10.1088/0022-3727/44/45/455305

[29] C. H. Ahn, Y. Y. Kim, D. C. Kim, S. K. Mohanta, and H. K. Cho. A comparative analysis of deep level emission in zno layers deposited by various methods. *Journal of Applied Physics*, 105:013502, 2009.
10.1063/1.3054175.

[30] D. da Silva Biron, V. dos Santos, and C. P. Bergmann. Synthesis and characterization of zinc oxide obtained by combining zinc nitrate with sodium hydroxide in polyol medium. *Materials Research*, 23:e20200080, 2020.
10.1590/1980-5373-MR-2020-0080

[31] X. Li, H. Zhu, J. Wei, K. Wang, E. Xu, Z. Li, and D. Wu. Determination of band gaps of self-assembled carbon nanotube films using tauc/davis-mott model. *Applied Physics A: Materials Science & Processing*, 97(2):341–345, 2009.
10.1007/s00339-009-5330-z

[32] A. Beer. Bestimmung der absorption des rothen lichts in farbigen flüssigkeiten. *Annalen der Physik*, 162(1):78–88, 1852.
10.1002/andp.18521620505

[33] J. H. Lambert. Photometry, or, on the measure and gradations of light intensity, colors, and shade. *Illuminating Engineering Society*, 1760.

[34] R. Jenkins, T. G. Fawcett, D. K. Smith, J. W. Visser, M. C. Morris, and L. K. Frevel. Jcpds—international centre for diffraction data sample preparation methods in x-ray powder diffraction. *Powder Diffraction*, 1(2):51–57, 1986.
10.1017/S0885715600011581

[35] D. Parajuli, G. C. Kaphle, N. Murali, and K. Samatha. Structural identification of cubic aluminum and non-cubic titanium using x-ray diffractometer. *Journal of Lumbini Engineering College*, 4(1):62–67, 2022.
10.3126/lecj.v4i1.49369

[36] W. L. B. M.A. Lxii. the crystalline structure of zinc oxide. *Transactions of the Faraday Society*, 39(0):647–650, 2009. 10.1080/14786440608636079

[37] J. Tom. Uv-vis spectroscopy: Principle, strengths and limitations and applications. *Tehnologija*, Network, Analysis and Separations, 2021.

[38] T. Namioka. Diffraction gratings. *Exp. Methods Phys. Sci.*, 31:347, 1998. 10.1016/B978-012617560-8/50018-9

[39] J. Tauc, R. Grigorovici, and A. Vancu. Optical properties and electronic structure of amorphous germanium. *Phys. Status Solidi*, 15:627, 1966. 10.1002/pssb.19660150224

[40] M. H. Habibi and M. K. Sardashti. Preparation of glass plate-supported nanostructure zno thin film deposited by sol-gel spin-coating technique and its photocatalytic degradation to monoazo textile dye. *J. Nanomater.*, 2008, 2008. 10.1155/2008/356765

[41] T. S. Shyju, S. Anandhi, R. Indirajith, and R. Gopalakrishnan. Solvothermal synthesis, deposition and characterization of cadmium selenide (cdse) thin films by thermal evaporation technique. *J. Cryst. Growth*, 337:38, 2011. 10.1016/j. jcrysgro.2011.09.051

[42] A. Smida, Z. Zaaboub, N. B. H. Mohamed, M. Hassen, F. Laatar, H. Maaref, and H. Ezzaouia. Photoluminescence behavior in the synthesized cdse thin films deposited on ito substrates. *J. Lumin.*, 194:686, 2018. 10.1016/j.jlumin.2017.09.036

[43] M. Nabil, I. V. P.-Quintana, M. Acosta, J. A. M. -Gamboa, and R. C.-Rodriguez. Morphological, structural, and optical bandgap characterization of extracted zno nanoparticles from commercial paste. *Adv. Mater. Sci. Eng.*, 2021, 2021. 10.1155/2021/9926544

[44] S. Datta, G. C. Kaphle, S. Baral, and A. Mookerjee. Study of morphology effects on magnetic interactions and band gap variations for 3d late transition metal bi-doped zno nanostructures by hybrid dft calculations. *The Journal of Chemical Physics*, 143(8):084309, 2015. 10.1063/1.4929510